Human Molecular Genetics, 2013, Vol. 22, No. 8 **1632–1642**
doi:10.1093/hmg/ddt013
Advance Access published on January 18, 2013

S/MAR-containing DNA nanoparticles promote persistent RPE gene expression and improvement in RPE65-associated LCA

Adarsha Koirala[1], Rasha S. Makkia[1], Shannon M. Conley[1], Mark J. Cooper[2] and Muna I. Naash[1,*]

[1]Department of Cell Biology, University of Oklahoma Health Sciences Center, 940 Stanton L. Young Boulevard, BMSB 781, Oklahoma City, OK 73104, USA and [2]Copernicus Therapeutics, Inc., Cleveland, OH 44106, USA

Received August 27, 2012; Revised January 7, 2013; Accepted January 14, 2013

Mutations in genes in the retinal pigment epithelium (RPE) cause or contribute to debilitating ocular diseases, including Leber's congenital amaurosis (LCA). Genetic therapies, particularly adeno-associated viruses (AAVs), are a popular choice for monogenic diseases; however, the limited payload capacity of AAVs combined with the large number of retinal disease genes exceeding that capacity make the development of alternative delivery methods critical. Here, we test the ability of compacted DNA nanoparticles (NPs) containing a plasmid with a scaffold matrix attachment region (S/MAR) and vitelliform macular dystrophy 2 (VMD2) promoter to target the RPE, drive long-term, tissue-specific gene expression and mediate proof-of-principle rescue in the *rpe65*$^{-/-}$ model of LCA. We show that the S/MAR-containing plasmid exhibited reporter gene expression levels several fold higher than plasmid or NPs without S/MARs. Importantly, this expression was highly persistent, lasting up to 2 years (last timepoint studied). We therefore selected this plasmid for testing in the *rpe65*$^{-/-}$ mouse model and observe that NP or plasmid VMD2-hRPE65-S/MAR led to structural and functional improvements in the LCA disease phenotype. These results indicate that the non-viral delivery of hRPE65 vectors can result in persistent, therapeutically efficacious gene expression in the RPE.

INTRODUCTION

Mutations in many genes expressed in the retinal pigment epithelium (RPE) cause debilitating degenerative diseases, including Leber's congenital amaurosis (LCA), Best's disease, retinitis pigmentosa and age-related macular degeneration (1,2). Although adeno-associated virus (AAV)-based vectors have been successful for ocular gene therapy (3–5), they are limited by their payload capacity which is <5 kb (6). Many therapeutic expression cassettes exceed this size, making the development of alternative therapeutic strategies extremely important. As a result, we have developed nanoparticles (NPs) comprising plasmid DNA compacted with lysine peptides conjugated to polyethylene glycol (CK30PEG) for gene delivery. These NPs can successfully incorporate DNA up to at least 20 kb (7) without a significant decrease in their transduction efficiency. We have shown that these NPs efficiently transfect both photoreceptors (8–10) and RPE cells (9,11) and can improve the disease phenotype in the *rds*$^{+/-}$ model of retinitis pigmentosa (8,10). They have been successfully used in the lung and the brain (12–17) and result in no toxic effects in the eye, even after repeated injections (10,18,19). Although our initial studies in the RPE demonstrated robust early NP-based gene expression, at longer timepoints, we observed a significant reduction in expression levels and a drop in the number of transduced RPE cells (11). To address this, we explored several genetic elements that have been used to improve the levels and the duration of exogenous gene expression in an effort to identify an improved plasmid vector for RPE targeting. Scaffold/matrix attachment regions (S/MARs) are one such element. S/MARs contain ~70% AT-rich regions (20) and have a high affinity for the nuclear matrix (21). When located directly the downstream of the expression cassette, S/MARs can help sustain enhanced gene expression in some systems (22). This is thought to occur by several mechanisms including transcriptional augmentation (23), episomal maintenance of plasmid DNA associated with the S/MAR (22) and insulator-like functions (23). These features make S/MAR elements attractive for the long-term

*To whom correspondence should be addressed. Tel: +1 4052712388; Fax: 4052713548; Email: muna-naash@ouhsc.edu

expression of non-viral vectors in RPE cells for which the persistence of gene expression is an ongoing challenge.

Here, we assessed the ability of an S/MAR-containing vector to generate persistent expression in RPE cells and the ability of this vector to mediate phenotypic improvement in the *rpe65*$^{-/-}$ model of LCA. We show that S/MAR-containing vectors, either NP-compacted or -uncompacted, can promote long-term (up to 2 years) elevated reporter gene expression in the RPE of wild-type (WT) mice. Furthermore, we show that this vector can be used to deliver the *hRPE65* gene and promote improvement in the LCA phenotype of *rpe65*$^{-/-}$ mice. These data suggest that vectors and NPs carrying S/MARs may provide a valuable non-viral approach for the genetic treatment of RPE-based diseases.

RESULTS

An S/MAR-containing vector exhibits enhances transgene expression levels in the RPE

We previously observed that expression from NP-VMD2 (vitelliform macular dystrophy 2)-eGFP peaked at post-injection day (PI)-2 and decreased up to PI-30, the longest timepoint studied (11). Our goal is persistent expression without a significant decrease over time, so we asked whether a different vector might yield improved persistence of expression. We chose to evaluate the pEPI vector (24–26), which contains an S/MAR. We generated constructs carrying the eGFP reporter gene under the control of the RPE-specific VMD2 promoter in either the peGFP backbone (11) or the pEPI backbone (with or without an S/MAR). The S/MAR in the pEPI vector is from the 5′ region of the human β-interferon gene and has been previously shown to enhance gene expression in CHO cells (22), hematopoietic stem cells *in vitro* (27) and liver tissue *in vivo* (28). After compacting the vectors into NPs, animals were subretinally injected in the superior central region with either 1 μl of NP (NP-VMD2-eGFP or NP-VMD2-eGFP-S/MAR; Supplementary Material, Fig. S1) or uncompacted naked DNA (VMD2-eGFP or VMD2-eGFP-S/MAR), at a concentration of 4.3 mg/ml. This concentration and volume has been previously shown to drive efficient retinal gene expression without causing toxicity (8–11,19). Control animals were either uninjected or vehicle (saline) injected.

We assessed gene expression at PI-2, PI-7, PI-30 and PI-120. The decrease in expression we previously observed for VMD2-eGFP (NPs and naked DNA) up to PI-30 (11) continued at PI-120: eGFP levels in NP-VMD2-eGFP-treated eyes at PI-120 were significantly reduced by 75% compared with levels at PI-2 ($P < 0.01$, by two-way analysis of variance (ANOVA) time/treatment, Fig. 1A). In contrast, there was no significant decrease in levels of expression from PI-2 to PI-120 in naked or NP-VMD2-eGFP-S/MAR-treated eyes (although means in NP-VMD2-eGFP-S/MAR were 25% lower at PI-120 than PI-2). Although there was no significant difference in expression between NP-VMD2-eGFP and NP-VMD2-eGFP-S/MAR at PI-2, the temporal decrease in eGFP expression in NP-VMD2-eGFP-treated eyes without a concomitant decrease in NP-VMD2-eGFP-S/MAR-treated eyes resulted in PI-120 levels which were 3.5-fold higher in NP-VMD2-eGFP-S/MAR- than NP-VMD2-eGFP-treated eyes (Fig. 1A). A similar trend was observed for naked VMD2-eGFP versus naked VMD2-eGFP-S/MAR: PI-120 levels were reduced by 87% (compared with PI-2) in VMD2-eGFP-treated eyes, but only reduced by 28% in VMD2-eGFP-S/MAR-treated eyes. NP-VMD2-eGFP-treated eyes exhibited eGFP levels significantly higher than VMD2-eGFP naked DNA-treated eyes at PI-2, but levels were not significantly different in NP-VMD2-eGFP-S/MAR versus VMD2-eGFP-S/MAR at any timepoint (although means were always lower in naked DNA-treated eyes than NP-treated eyes).

As expected, eGFP expression was limited to the RPE layer (Fig. 1B–E) after treatment with any vector/NP. Co-localization is detected between eGFP and the RPE cell marker RPE65 (red, Fig. 1D), but not between eGFP and the photoreceptor marker RDS (red, Fig. 1C) in all groups (Fig. 1B–D shows a naked VMD2-eGFP-S/MAR-treated eye, all groups shown in Fig. 1E).

We next assessed the extent to which eGFP was distributed throughout the retina at PI-120. eGFP-positive cells were detected in all cohorts except saline via *in vivo* fundus imaging (Fig. 1F), and the examination of RPE whole mounts (Fig. 1G). Fundus images suggested that expression from S/MAR-containing vectors was more widely distributed than that from non-S/MAR vectors and that the retinal distribution is enhanced for NPs compared with naked DNA. Next, a blinded observer scored the percentage of cells expressing eGFP in RPE whole mounts. eGFP-expressing cells were detected in all quadrants (Fig. 1H), indicating that expression was not limited to the region of injection. Significantly more eGFP-expressing cells were detected in eyes injected with S/MAR-containing vectors; in the superior quadrant, 40% (naked) and 50% (NP) of cells in S/MAR-injected eyes expressed eGFP, while only 8% (naked) and 20% (NP) of cells expressed eGFP in eyes injected with non-S/MAR vectors (Fig. 1H, $^{**}P < 0.01$, $^{***}P < 0.001$). There were no significant differences between NP and naked DNA-treated eyes (either plasmid) in any quadrant. A similar trend was seen in all other quadrants. Although expression was not limited to the region of injection, the highest number of expressing cells was detected in the superior quadrant (consistent with injection in the superior central region), with the mean number of eGFP-positive cells following the trend superior > nasal > temporal > inferior for all groups. Supplementary Material, Figure S2 shows data from Figure 1H replotted to illustrate these quadrant-based differences. Interestingly, although there was no statistically significant difference between the percent of eGFP-expressing cells in each quadrant in NP-VMD2-eGFP-S/MAR and VMD2-eGFP-S/MAR (Fig. 1H), it appears that NP-VMD2-eGFP-S/MAR has a slightly broader distribution throughout the retina compared with VMD2-eGFP-S/MAR: as shown in Supplementary Material, Figure S2A, NP-VMD2-eGFP-S/MAR-treated eyes exhibited no statistically significant decrease in the number of cells expressing GFP between the superior and nasal quadrants (GFP-positive cells in the temporal and inferior quadrants were significantly fewer than those in the superior

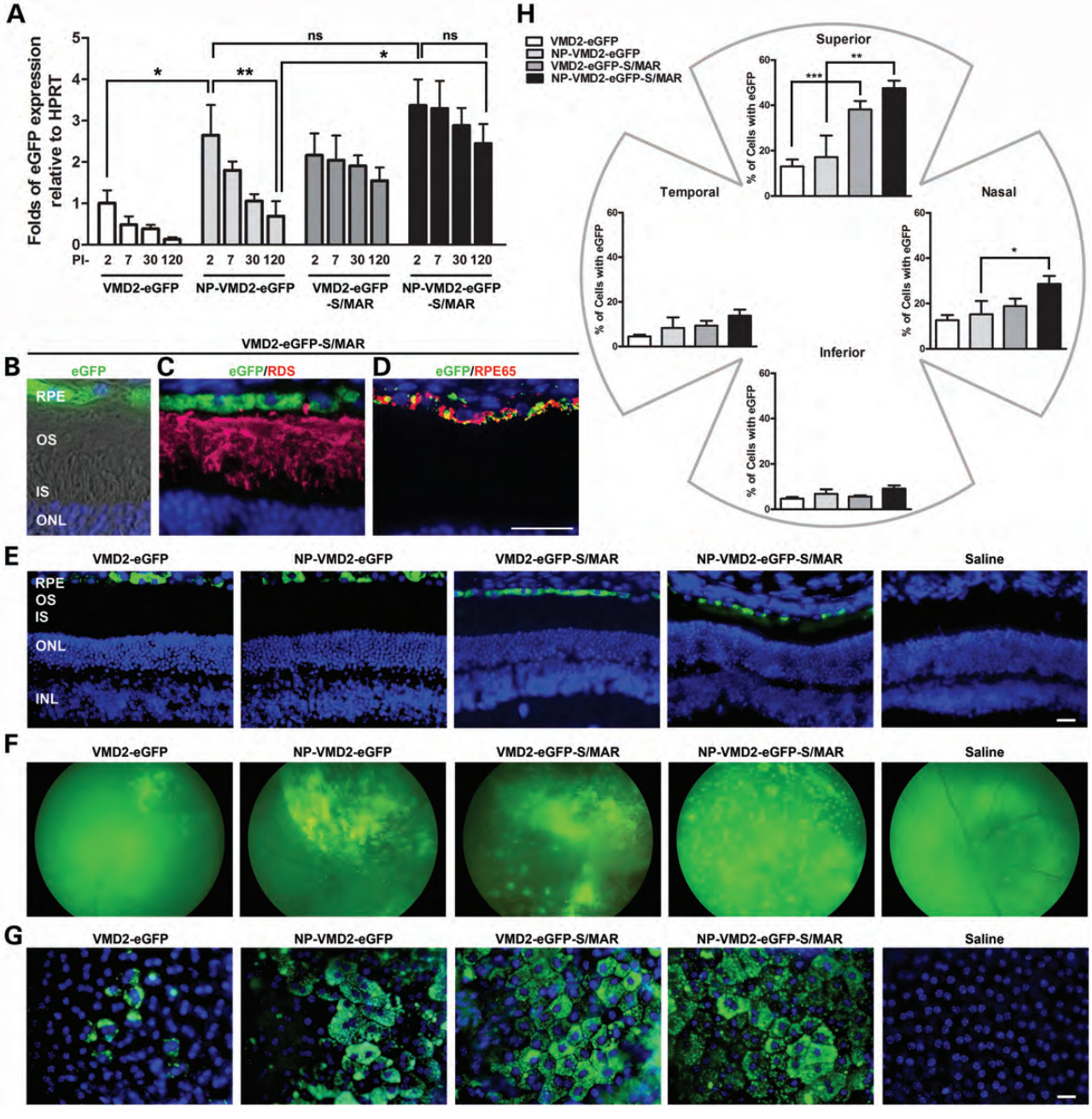

Figure 1. S/MAR vectors drive retinal gene expression. (**A**) Quantitative real-time PCR (qRT-PCR) analysis was conducted at PI-2, PI-7, PI-30 and PI-120 on whole eyes from WT animals after P30 injection of the indicated vectors. eGFP levels were normalized to the housekeeping gene HPRT. $^{*}P < 0.05$ and $^{**}P < 0.01$ in two-way ANOVA with Bonferroni's *post hoc* test. All significant pairwise comparisons are shown. PI-2, PI-7 and PI-30 data for VMD2 eGFP and NP-VMD2-eGFP are replotted from (11). Experiments were conducted under the same conditions and by the same person here as in (11), and HPRT values were consistent across timepoints. (**B**–**D**) Cryosection taken at PI-120 from an animal injected with VMD2-eGFP-S/MAR. (B) Native eGFP fluorescence, DAPI and Nomarski. (C) IHC of the same eye as (B) showing single planes with eGFP, DAPI and anti-RDS labeling (red). (D) IHC showing eGFP and anti-RPE65 labeling (red). (**E**) Representative images showing native eGFP fluorescence in the RPE. (**F**) Fundus images showing the distribution of eGFP expression at PI-120. (**G**) Native eGFP fluorescence in representative RPE whole mounts at PI-120. (**H**) eGFP-positive cells at PI-120 were counted in six 20× images from each quadrant. Values were summed and expressed as a fraction of the total number of RPE cells counted (6000–7000 cells counted per eye). $^{*}P < 0.05$, $^{**}P < 0.01$ and $^{***}P < 0.001$ by one-way ANOVA with Bonferroni's *post hoc* test. All significant comparisons are shown. $n = 3$–4 eyes/group for each experiment. Scale bar: B–D, 10 μm; E and G, 20 μm. RPE, retinal pigment epithelium; OS, outer segment; IS, inner segment; ONL, outer nuclear layer; INL, inner nuclear layer.

quadrant). In contrast, there was a striking, statistically significant drop in GFP-positive cells from the superior quadrant to all other quadrants in VMD2-eGFP-S/MAR-treated eyes (Supplementary Material, Fig. S2A). Overall, our results indicate that at PI-120 ∼21% of all RPE cells express eGFP in the eyes treated with S/MAR-containing vectors.

S/MAR-containing vectors generate long-term transgene expression in the RPE

Given the positive data with S/MAR containing vectors at PI-120, we selected this vector for long-term testing. eGFP mRNA levels from S/MAR NPs remained detectable up to

the longest timepoint tested (PI-360, Fig. 2A) with no significant decrease in expression compared with PI-120 (Fig. 2A). Interestingly, the uncompacted S/MAR vector drove persistent gene expression in addition to the NP-compacted vector, although on average mRNA expression levels from the uncompacted vector were lower (not statistically significant) than NPs. As at other timepoints, at PI-360, eGFP expression was in RPE cells; observe the co-localization of eGFP (green) with immunolocalization of RPE65 (red) in an RPE whole mount in Figure 2B (shown for NP-VMD2-eGFP-S/MAR). Fundus images collected at PI-360 (Fig. 2C) confirm the continued expression of eGFP in a pattern similar to that observed at PI-120. To assess the distribution at long timepoints, eGFP-positive cells were quantified in RPE whole mounts (Fig. 2D) at PI-720 (PI-2 years). At PI-2 years, expression was seen throughout the RPE cell layer, but with a larger percent of expressing cells in the superior quadrant (38.8 and 44.4% for naked and NP, respectively) compared with the other quadrants (Fig. 2E). There was no significant drop in the percent of eGFP-expressing cells from PI-120 to PI-2 years, and at PI-2 years, there was no statistically significant difference in any quadrant between naked and NP-treated eyes. Finally, whole mounts from eyes collected at PI-2.5 years were examined and they too exhibited tissue-wide eGFP expression similar to that seen at the 2-year timepoint (Supplementary Material, Fig. S3). These results indicate that S/MAR-based vectors mediate the sustained expression of reporter genes in the RPE.

S/MAR-containing vectors generate improvement in the LCA phenotype in *rpe65*$^{-/-}$ mice

Given the favorable expression profile of the S/MAR-containing vectors, we elected to use them for phenotypic rescue studies in an RPE disease model. The logical choice was the *rpe65*$^{-/-}$ murine model of LCA which has been commonly used for gene therapy studies (29–31). The human *RPE65* cDNA was cloned into the S/MAR vector in the place of eGFP and after compaction was subretinally injected in *rpe65*$^{-/-}$ mice. Mice were treated at postnatal day 16, since early treatment has provided better improvements in LCA phenotypes (32,33). Since the S/MAR-containing vectors drove long-term reporter gene expression in the RPE, we assessed phenotypes at PI-180. *RPE65* message levels were assessed using primers that amplified from both mouse and human orthologs. *RPE65* message levels in the eyes treated with naked (plasmid, p-) or NP-VMD2-hRPE65-S/MAR were ~50% of WT levels (Fig. 3A). There were no statistically significant differences between levels of expression in NP-VMD2-hRPE65-S/MAR-treated eyes compared with VMD2-hRPE65-S/MAR-treated eyes. In common with other studies (34), we observe no stable *RPE65* message in uninjected *rpe65*$^{-/-}$ mice. Immunolabeling with antibodies against human/mouse RPE65 (green) showed that, as expected, expression was restricted to the RPE (Fig. 3B).

To determine whether this expression-mediated improvements in the LCA phenotype, RPE structure and retinal function were evaluated at PI-180. At this age, untreated *rpe65*$^{-/-}$ mice exhibit several structural phenotypes including: (i) reduced outer nuclear layer (ONL) thickness, (ii) reduced cone number (35), (iii) accumulation of lipid-like droplets in the RPE cells (34), (iv) expansion of RPE basal infoldings into the RPE cytosol (36) and (v) increased fundus albipunctatus phenotype (37).

Morphometric analysis of central retinal sections collected from both naked DNA and NP-injected eyes showed improved ONL thickness in the superior central region at PI-180 (Fig. 3C and D, significant differences between WT/uninjected-*, uninjected/NP-hRPE65-+ and uninjected/p-hRPE65-^), but not in the inferior region, consistent with the distribution of expression we observed with the eGFP vectors. There were no significant differences in ONL thickness between NP-VMD2-hRPE65-S/MAR-treated eyes and VMD2-hRPE65-S/MAR-treated eyes. Next, the number of cones in 4 fields from each quadrant (16 fields per eye at 20 times magnification) was counted from retinal flatmounts labeled with antibodies against short wavelength (SWL) cone opsin (red, Fig. 3F) and medium wavelength (MWL) cone opsin (green, Fig. 3F) and then averaged to give an overall value representing the number of remaining cones across the whole retina. In keeping with the structural improvement in the ONL, treatment with NPs resulted in the significant preservation of both MWL and SWL cones (Fig. 3E and F), while naked DNA treatment resulted in the significant preservation of MWL cones compared with saline treatment ($^{*}P < 0.05$).

We next examined the accumulation of lipid droplets, appearance of white fundus spicules (a fundus albipunctatus phenotype), RPE basal infoldings and Bruch's membrane. The number and size of lipid droplets in the RPE at PI-180 was assessed by a blinded observer in 10–15 images per eye collected along the inferior–superior plane (Fig. 3G, arrows in Fig. 3H, $n = 4–5$ eyes/group). Treatment with VMD2-hRPE65-S/MAR naked DNA or NPs resulted in a reduction in the RPE area occupied by lipid droplets (Fig. 3G, top) and fewer lipid-like droplets overall (Fig. 3G, bottom) when compared with untreated eyes, although the differences were not statistically significant. In addition, we observed a reduction in the appearance of white dots (arrows, Fig. 3I) in the fundus images of NP and naked VMD2-hRPE65-S/MAR-treated animals at PI-180 (Fig. 3I, Supplementary Material, Fig. S4). Consistent with the distribution of gene expression, this reduction in the white dot phenotype was most pronounced in the superior region; observe the white spots in the inferior region of the naked VMD2-hRPE65-S/MAR fundus (Fig. 3I, arrowhead). Normally, the RPE exhibits lobular basal infoldings (boxes, Supplementary Material, Fig. S5) protruding toward Bruch's membrane. In the absence of RPE65, these infoldings begin to protrude abnormally into the RPE cytoplasm and exhibit a more thread-like appearance (Supplementary Material, Fig. S5, red arrows), a defect not observed in DNA and NP-treated eyes (Supplementary Material, Fig. S4).

Functionally, *rpe65*$^{-/-}$ mice exhibit minimal or no scotopic retinal function, reduced MWL green-cone signal and extinguished SWL UV-cone signals (34,38). Although no significant improvement was observed in the scotopic a-wave in treated animals (Fig. 4A and C, left panel), scotopic b-waves were improved in NP and naked DNA-treated animals compared with controls ($^{*}P < 0.05$, Fig. 4C, right panel) at PI-180. Importantly, at PI-180, NP and naked DNA-treated eyes exhibited significantly higher green photopic b-wave (a

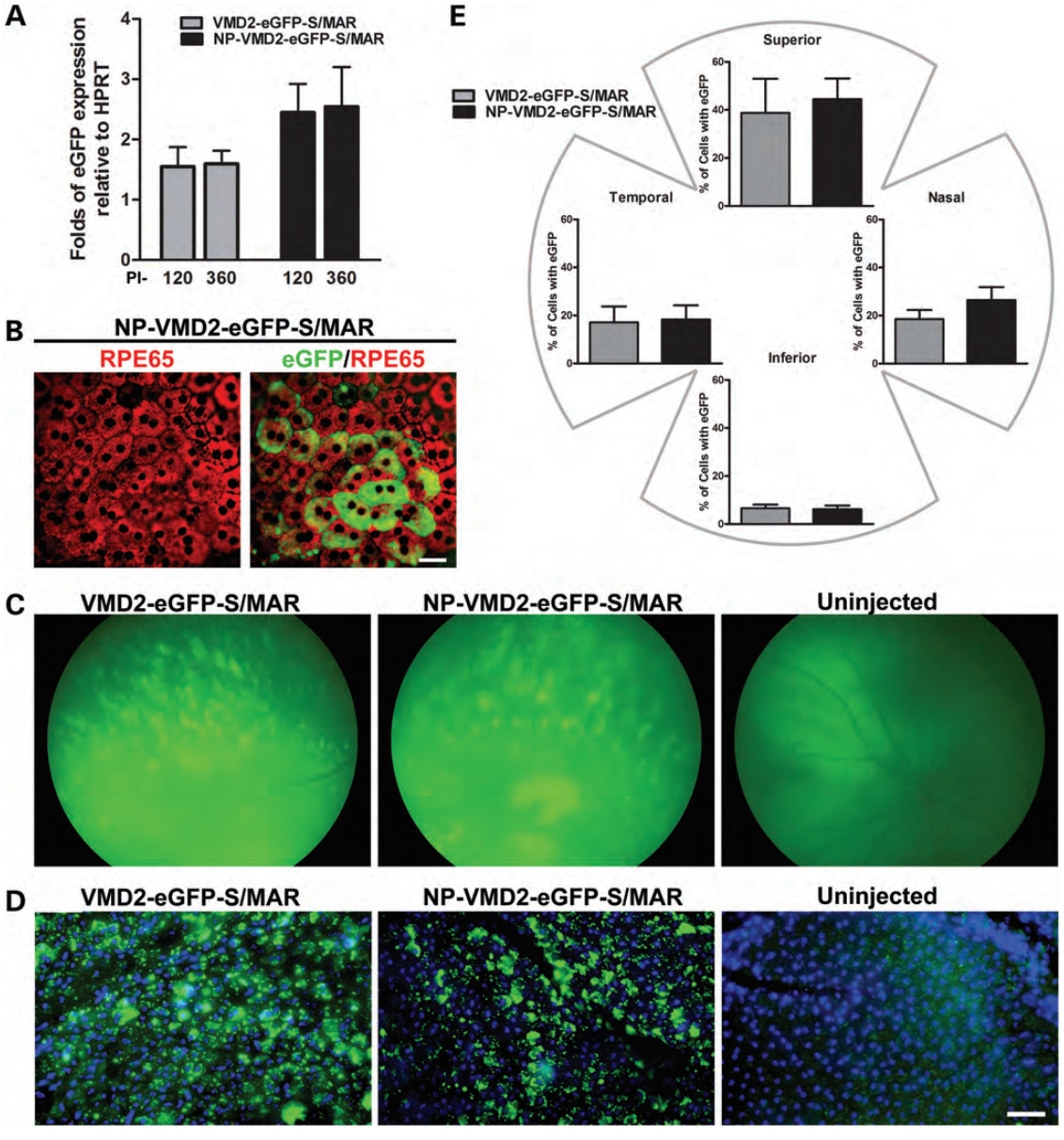

Figure 2. S/MAR-containing vectors drive retinal gene expression for up to 2 years. (**A**) qRT-PCR was conducted on whole eyes injected with S/MAR-containing vectors ($n = 5–8$/group) at PI-360, PI-120 results from Figure 1A shown for comparison. (**B**) PI-360 RPE whole mounts labeled with antibodies against RPE65 (red) and native eGFP fluorescence. (**C**) Fundus images showing eGFP expression at PI-360. (**D**) RPE whole mounts showing native eGFP fluorescence with DAPI at PI-2 years. (**E**) eGFP-positive cells were counted in six images (×20 magnifications) from each quadrant of injected eyes at PI-2 years. Values were summed and expressed as a fraction of the total number of RPE cells counted. There were no significant differences between naked DNA and NP injections in all quadrants ($P > 0.05$). Scale bar: (B) 10 μm; (D) 50 μm.

measure of MWL cone function) and UV photopic b-wave (a measure of SWL cone function) amplitudes compared with saline-treated animals ($^{**}P < 0.01$ and $^{*}P < 0.05$, Fig. 4D). Improvement in MWL cone function was particularly robust, with green b-wave amplitudes 71 and 79% of WT in DNA and NP VMD2-hRPE65-S/MAR-treated eyes, respectively. Although SWL cone function was improved by 2–3-fold in treated eyes, UV b-wave amplitudes in DNA- and NP-treated animals were only 21 and 25% of WT, respectively. These results are consistent with our morphometric studies which showed better improvement in MWL cones than SWL cones (Fig. 3E). There were no significant differences in any functional parameters between NP- and naked DNA-injected animals. Overall, these data show that S/MAR containing vectors, either NP compacted or uncompacted, can generate significant structural and functional improvement in the *rpe65*$^{-/-}$ LCA phenotype.

DISCUSSION

The *rpe65*$^{-/-}$ mouse and other RPE65 mutant disease models have been extensively used to test a variety of gene therapy vectors, including AAVs (3–5,32,39). While AAVs may be a good option for the treatment of RPE65-associated LCA,

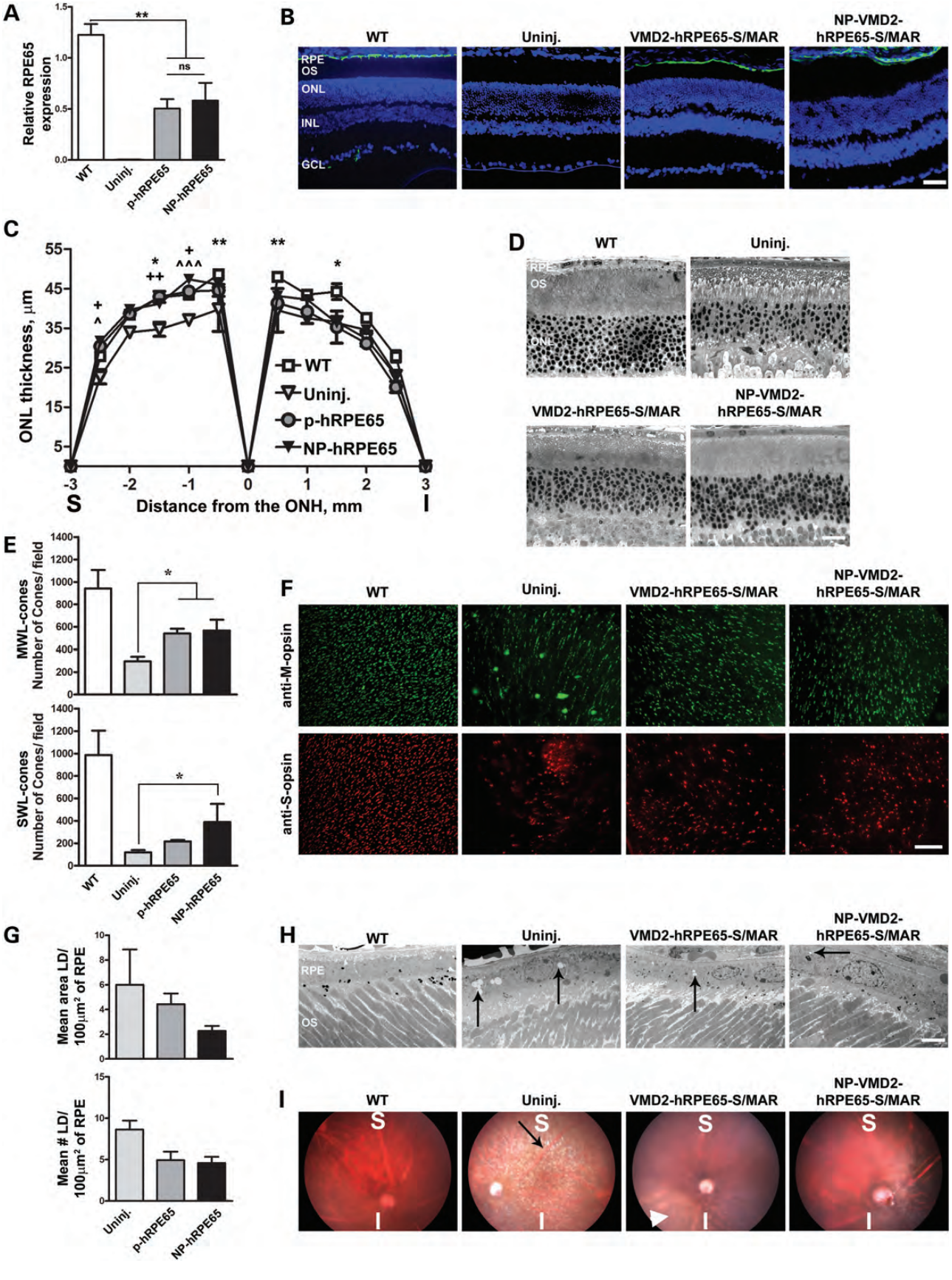
A
Relative RPE65 expression
1.5
1.0
0.5
0.0
**
ns
WT
Uninj.
p-hRPE65
NP-hRPE65
B
WT
Uninj.
VMD2-hRPE65-S/MAR
NP-VMD2-hRPE65-S/MAR
RPE
OS
ONL
INL
GCL
C
ONL thickness, μm
55
45
35
25
15
5
-3
-2
-1
0
1
2
3
S
Distance from the ONH, mm
I
WT
Uninj.
p-hRPE65
NP-hRPE65
D
WT
Uninj.
RPE
OS
ONL
VMD2-hRPE65-S/MAR
NP-VMD2-hRPE65-S/MAR
E
MWL-cones Number of Cones/ field
SWL-cones Number of Cones/ field
1400
1200
1000
800
600
400
200
0
WT
Uninj.
p-hRPE65
NP-hRPE65
F
WT
Uninj.
VMD2-hRPE65-S/MAR
NP-VMD2-hRPE65-S/MAR
anti-M-opsin
anti-S-opsin
G
Mean area LD/ 100μm² of RPE
Mean # LD/ 100μm² of RPE
10
8
6
4
2
0
15
10
5
0
Uninj.
p-hRPE65
NP-hRPE65
H
WT
Uninj.
VMD2-hRPE65-S/MAR
NP-VMD2-hRPE65-S/MAR
RPE
OS
I
WT
Uninj.
VMD2-hRPE65-S/MAR
NP-VMD2-hRPE65-S/MAR
S
I

many ocular disease genes are too large for AAVs. Neither delivery option we study here (naked DNA or compacted NPs) has defined size limitations. Our unimolecularly compacted DNA NPs have shown no loss of transduction efficiency in the lung with plasmids up to 20 kb (largest size tested) (7), and we have used DNA NPs carrying a 14 kb plasmid to target photoreceptors and mediate phenotypic rescue in the *Abca4*$^{-/-}$ model of Stargardt's disease (40). Our work here shows that for RPE targeting, effective long-term gene expression can be obtained with naked or nanocompacted S/MAR-containing plasmids. This longevity of expression is critical for the treatment of chronic disease in post-mitotic tissues and has not previously been shown in the RPE using non-viral vectors. Interestingly, a main limitation we found was that only ∼20% of RPE cells expressed the transduced gene. While expressing cells were distributed throughout the retina, they were most concentrated in the region of injection. Gene expression levels were high (∼50% of WT in treated *rpe65*$^{-/-}$ mice), suggesting that individual cells are expressing the transduced gene at levels near or exceeding the WT level and that future studies will need to focus on expanding the distribution of gene expression.

A main feature of our results is that throughout the current studies, we did not observe any statistical difference between the outcomes in S/MAR-based naked DNA- versus NP-treated eyes. This is in striking contrast to our work in photoreceptors in which we have seen that uncompacted S/MAR-containing vectors do not generate gene expression or mediate phenotypic rescue nearly as well as their nanocompacted counterparts (40). Thus, there are two distinct questions here: (i) why is the naked S/MAR vector as effective as the nanocompacted S/MAR vector at RPE targeting and (ii) why does the naked S/MAR-containing vector generate better gene expression than the naked non-S/MAR vector? We hypothesize that equivalent efficacy of nanocompacted versus naked is due to the phagocytic activity of the RPE. RPE cells are highly phagocytic in nature (41), a physiological feature which facilitates non-specific uptake but is not shared by photoreceptors. NPs transfect some cells by a nucleolin-mediated specific uptake pathway (42,43), and their robust uptake into non-phagocytic cells, such as photoreceptors, is thought to depend on this process.

The increased persistence of the expression of the S/MAR containing vectors compared with the non-S/MAR vectors is likely due to the ability of the S/MAR to increase DNA persistence in the nucleus and increased localization to active regions of the nucleus, two well-established features of S/MARs. Increased gene expression from S/MAR-containing vectors has been hypothesized to be based on position effects and increased stability of the message (22,23). It has also been shown *in vitro* that the positioning of S/MAR immediately downstream of the expression cassette is required for episomal maintenance (22), a favorable feature for gene therapy compared with random integration. Overall, our data showing the maintenance of RPE transgene expression for the life of the animal significantly enhance the clinical relevance of non-viral gene therapy for chronic ocular diseases.

Here, have identified a plasmid vector which can mediate persistent gene expression and can mediate improvement in a disease model, a critical step for new therapeutic tools. We observe that treated *rpe65*$^{-/-}$ mice exhibited improvements in ONL thickness, improvements in scotopic and photopic ERGs, reduction in the white dot fundus phenotype and a reduced (although non-significant) accumulation of lipid droplets compared with control eyes. These phenotypes are due to the accumulation of retinyl esters as a result of lack of RPE65 isomerohydrolase activity, and their attenuation suggests that the delivered hRPE65 is functional. These results are further supported by our Supplementary data showing that treatment results in a reduction in the extension of basal infoldings into the RPE cytoplasm (an indicator of RPE atrophy) and increased retinal health (preservation of cones).

These phenotypes correlate with loss of vision (34) and we observed the significant preservation of cone function. While we were surprised by the lack of improvement in the scotopic ERGs, the refractory nature of this phenotype has been well-documented (31,44) and may be due to decreased synthesis of 11-cis retinal in these mice (37). In support of this hypothesis, the administration of 9-cis retinal (precursor for the visual chromophore) has led to improvements in scotopic ERG (45), suggesting that a combinatorial approach of dietary supplementation and gene therapy may yield optimal results. A combinatorial approach consisting of gene replacement therapy and oral delivery of retinoid precursors has shown to yield a significant improvement in the rod vision in another LCA model with defects in retinoid processing (*lrat*$^{-/-}$) (46).

In conclusion, we here report that naked or compacted DNA incorporating eGFP cDNA results in elevated, prolonged (2.5 years) gene expression in the RPE and that these vectors, when encoding *hRPE65*, can mediate phenotypic improvement in *rpe65*$^{-/-}$ mice. Previously, we also demonstrated the safety

Figure 3. S/MAR-containing *hRPE65* vectors mediate improvement in structural phenotypes in the *rpe65*$^{-/-}$ model. (**A**) qRT-PCR was conducted at PI-180 on whole eyes from *rpe65*$^{-/-}$ animals injected at P16 with S/MAR-containing *hRPE65* vectors using primers that amplify from both mouse and human *RPE65*. $^{**}P < 0.01$ by one-way ANOVA with Bonferroni's *post hoc* comparison. (**B**) IHC showing the distribution of RPE65 (green) at PI-180 in *rpe65*$^{-/-}$ mice using Abcam antibody 13826 against human and mouse RPE65. (**C**) ONL thickness was measured at PI-180 at increasing distances from the optic nerve head (ONH). Asterisk indicates significant differences between WT and uninjected, plus symbol indicates significant differences between NP and uninjected, arrow head symbol indicates significant differences between naked and uninjected. One symbol, $P < 0.05$, two symbols, $P < 0.01$, three symbols $P < 0.001$ by two-way ANOVA with Bonferroni's *post hoc* tests. $n = 3–5$ eyes/group. (**D**) Representative images used for quantification in (C). (**E** and **F**) PI-180 retinal whole mounts were labeled with antibodies against MWL cone opsin (upper panels F, green) and SWL cone opsin (lower panels F, red). Cones were counted in 16 images (four/quadrant) from each eye using ImageJ. Values were averaged to give mean cone counts/field for the whole eye. $n = 4$ eyes/group. Shown in (E) are the mean ± SEM. $^{*}P < 0.05$ in one-way ANOVA with Bonferroni's *post hoc* test. (**G** and **H**) RPE lipid droplets (arrows, H) were counted and their area measured in 10–15 EM images/eye (4 eyes/group) at PI-180. Representative EMs shown in (H). The mean area occupied by the lipid droplets/100 μm^2 of RPE is shown in the top panel of (G), while the mean number of lipid droplets/100 μm^2 of RPE is shown in the bottom panel of (G) (± SEM). (**I**) Fundus images were obtained at PI-180 showing improvement in lipid droplet accumulation at the region of injection. Black arrow shows white spicules indicative of retinyl ester accumulation; white arrowhead shows the same phenotype in the inferior of a VMD2-hRPE65-S/MAR-treated eye. Scale bars: (B) 40 μm; (D) 20 μm; (F) 50 μm; (H) 200 nm. RPE, retinal pigment epithelium; OS, outer segment; IS, inner segment; ONL, outer nuclear layer; INL, inner nuclear layer; GCL, ganglion cell layer.

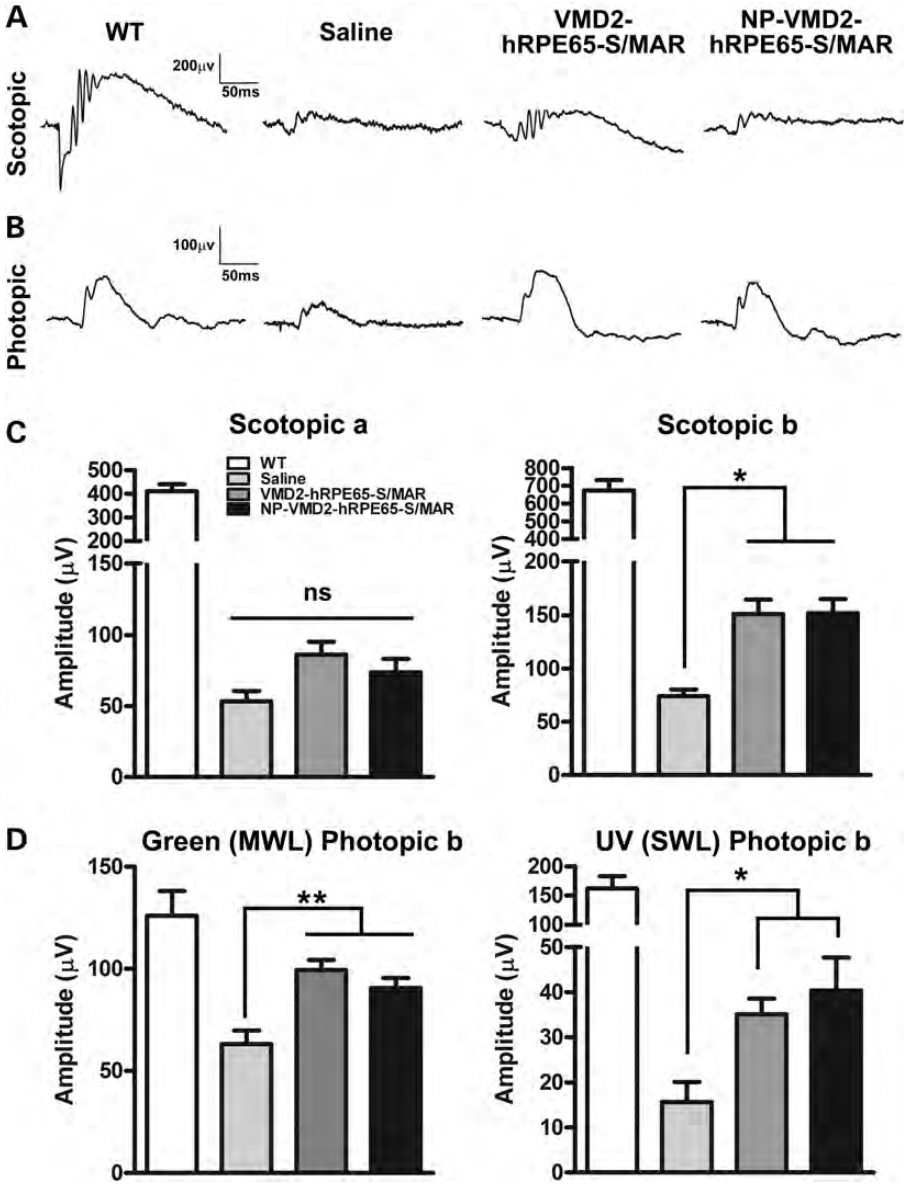

Figure 4. S/MAR-containing *hRPE65* vectors mediate improved cone function in *rpe65*$^{-/-}$ mice. Full-field scotopic (**A**) and photopic (**B**, white light) ERG was performed at PI-180. (**C**) Mean scotopic a-wave (left) and b-wave (right) amplitudes (±SEM). (**D**) Mean photopic b-wave amplitudes (±SEM) recorded in response to green (left, MWL cones) or UV (right, SWL cones) light. $^{*}P < 0.05$ and $^{**}P < 0.01$ in one-way ANOVA with Bonferroni's *post hoc* test. $n =$ 7–15 eyes/group.

of similar vectors in both single and repeat injections (10,18,47). These data suggest that S/MAR containing DNA and NPs may be an excellent addition to the available repertoire of clinically feasible treatments for RPE-based disorders.

MATERIALS AND METHODS

Plasmid DNA construction and NP compaction

The human VMD2 promoter (−585/+38) was cloned into pEGFP-1 (Invitrogen, CA, USA) and the pEPI-eGFP vector containing an S/MAR (Supplementary Material, Fig. S1) generously shared by Dr Isa Stehle/Dr Hans Lipps (University of Witten/Herdecke) (24–26). In some experiments, eGFP was replaced by hRPE65 cDNA (Supplementary Material, Fig. S1). Purified, endotoxin-free plasmid was compacted into NPs as previously described using acetate as the lysine counterion (7,48). After initial formulation, NPs were concentrated to 4.3 mg/ml in saline.

Animal care and subretinal injections

Animal experiments were approved by the Institutional Animal Care and Use Committee (University of Oklahoma, Oklahoma City, USA) and were performed under the guidelines of the Association of Research in Vision and Ophthalmology (Rockville, MD, USA). WT Balb/c and *rpe65*$^{-/-}$ mice were maintained under cyclic light (12L-30 lux:12D) conditions. Fundus

imaging experiments using *rpe65*$^{-/-}$ mice were done on mice in the agouti background; however, all other experiments were conducted on albino mice (either *rpe65*$^{-/-}$ or WT). Subretinal injections were performed as described previously (11) at either P30 (Balb/c) or P16 (*rpe65*$^{-/-}$). Subretinal injections were trans-corneal in all animals used for quantitative real-time PCR (qRT-PCR) and native fluorescence. To minimize corneal and lens opacification that can interfere with *in vivo* imaging, for fundus photography, subretinal injections were trans-scleral. Briefly, all injections were performed with 1 μl of 4.3 mg/ml DNA or NPs. Both trans-scleral and trans-corneal injections delivered the material at the superior-nasal portion of the mouse eye. Injection was performed by a single individual at ∼85% success rate.

Quantitative real-time PCR

qRT-PCR was performed and data were analyzed as described previously (11). eGFP levels and RPE65 levels were normalized to the housekeeping gene HPRT. Primers used in these experiments are in Supplementary Material, Table S1. The experimental data set that has been replotted in Figure 1 and other data sets were performed and analyzed by same individual. HPRT values were consistent throughout all experiments. RPE65 mRNA was undetectable in the *rpe65*$^{-/-}$ animals by RT-PCR using the primers mentioned in Supplementary Material, Table S1.

Immunohistochemistry

Immunohistochemistry was performed as described previously (11). Retinal cryosections or whole mounts were blocked and incubated overnight with antibodies against human and mouse RPE65 (Abcam, ab13826, 1:300), mouse RPE65 (shared by Dr J. Ma, 1:500), GFP (Invitrogen, A11122, 1:1000), RDS-CT (generated in- house against the C-terminal of RDS, 1:1000) (49), Lamin B1 (Santa Cruz, sc-20682, 1:300), S-opsin (Santa Cruz, sc-14363, 1:500) or M-opsin (generously shared by Dr. Cheryl Craft, 1:25 000) (50). Images were acquired with a BX-62 spinning disk confocal microscope (Olympus). For experiments in which eGFP-positive cells were counted, only cells exhibiting robust eGFP signal throughout the cytoplasm were counted: cells with a spotted pattern were not considered positive. Images for the quantification of these cells were taken at 20× magnification.

Electroretinography

Mice were dark adapted overnight, anesthetized and electroretinography (ERG) was performed as described previously (49). Briefly, a stimulus intensity of 2.13 log cd s/m^2 was presented to dark-adapted, dilated eyes in a ganzfeld (Model GS-2000; LKC Technologies, Gaithersburg, MD, USA) to record scotopic a- and b-wave responses. Photopic responses were evaluated after a 5 min light adaptation at 1.46 log cd s/m^2. Photopic measurements are averages of 25 strobe flashes of white light (1.89 log cd s/m^2), green light (510 nm peak, 1.09 log cd s/m^2) or UV light (360 nm peak, −0.10 log cd s/m^2). Amplitudes are presented as the mean ± SEM.

Fundus imaging

Fundus imaging was performed as described previously (11). Briefly, mice were anesthetized, placed on a pedestal and the eye was placed under the lens of the MICRON III camera (Phoenix Laboratories). Images were taken using brightfield or GFP filters. Gain function in the camera controller was assigned the maximum value for images taken with the GFP filter (excitation, 482 nm, emission, 536 nm). Fundus images were captured at equal exposure times. Background correction involved removing all signal below a threshold intensity from each image. This threshold was the same for all images and does not impact interpretation of the data.

Transmission electron microscopy

Electron micrographs of NPs (7,48) and retinal sections (8) were prepared as described previously. Lipid droplets were manually counted from 10 to 16 EMs per eye (cut superior-inferior) and 4–5 animals for each cohort. The area occupied by the RPE and the lipid droplets in the EMs were calculated using Adobe Photoshop CS3.

Retinal morphometry and ONL thickness measurements

About 10–14 40× images were taken from all cohorts starting from the optic nerve head at an interval of 0.5 mm. ONL thickness was measured in Adobe Photoshop CS3 from three sections each and averaged for each data point. For each cohort, images were taken along the vertical meridian-superior and inferior to the optic nerve head.

Statistical analyses

Statistics were performed as indicated in each figure using one-way or two-way ANOVA with Bonferroni's *post hoc* comparisons as necessary for each experiment. All results are two-tailed with significance defined at a *P*-value of <0.05.

SUPPLEMENTARY MATERIAL

Supplementary Material is available at *HMG* online.

ACKNOWLEDGEMENTS

The authors thank Barbara Nagel and Jan Ryerse from St Louis University for the EM imaging. We thank Drs Hans Lipps and Isa Stehle for the pEPI vector. The M-opsin and RPE65 antibodies were generously provided by Dr Cheryl Craft (University of Southern California) and Dr J.X. Ma (University of Oklahoma HSC), respectively. Dr Michael Redmond (National Eye Institute) shared the *rpe65*$^{-/-}$ mice.

Conflict of Interest statement. M.J.C. is an employee of Copernicus Therapeutics, Inc. and owns stock in the company.

FUNDING

This work was supported by the National Eye Institute (EY10609 to M.I.N., EY018656 to M.I.N., EY018512 to S.M.C.), the Foundation Fighting Blindness (M.I.N.), the Oklahoma Center for the Advancement of Science and Technology (S.M.C. and M.I.N.) and the state of Ohio Biomedical Research Commercialization Program (M.J.C.).

REFERENCES

1. Travis, G.H., Golczak, M., Moise, A.R. and Palczewski, K. (2007) Diseases caused by defects in the visual cycle: retinoids as potential therapeutic agents. *Annu. Rev. Pharmacol. Toxicol.*, **47**, 469–512.
2. Xiao, Q., Hartzell, H.C. and Yu, K. (2010) Bestrophins and retinopathies. *Pflugers Arch.*, **460**, 559–569.
3. Bainbridge, J.W., Smith, A.J., Barker, S.S., Robbie, S., Henderson, R., Balaggan, K., Viswanathan, A., Holder, G.E., Stockman, A., Tyler, N. *et al.* (2008) Effect of gene therapy on visual function in Leber's congenital amaurosis. *N. Engl. J. Med.*, **358**, 2231–2239.
4. Cideciyan, A.V., Aleman, T.S., Boye, S.L., Schwartz, S.B., Kaushal, S., Roman, A.J., Pang, J.J., Sumaroka, A., Windsor, E.A., Wilson, J.M. *et al.* (2008) Human gene therapy for RPE65 isomerase deficiency activates the retinoid cycle of vision but with slow rod kinetics. *Proc. Natl Acad. Sci. USA*, **105**, 15112–15117.
5. Maguire, A.M., Simonelli, F., Pierce, E.A., Pugh, E.N. Jr, Mingozzi, F., Bennicelli, J., Banfi, S., Marshall, K.A., Testa, F., Surace, E.M. *et al.* (2008) Safety and efficacy of gene transfer for Leber's congenital amaurosis. *N. Engl. J. Med.*, **358**, 2240–2248.
6. Wu, Z., Yang, H. and Colosi, P. (2010) Effect of genome size on AAV vector packaging. *Mol. Ther.*, **18**, 80–86.
7. Fink, T.L., Klepcyk, P.J., Oette, S.M., Gedeon, C.R., Hyatt, S.L., Kowalczyk, T.H., Moen, R.C. and Cooper, M.J. (2006) Plasmid size up to 20 kbp does not limit effective *in vivo* lung gene transfer using compacted DNA nanoparticles. *Gene Ther.*, **13**, 1048–1051.
8. Cai, X., Nash, Z., Conley, S.M., Fliesler, S.J., Cooper, M.J. and Naash, M.I. (2009) A partial structural and functional rescue of a retinitis pigmentosa model with compacted DNA nanoparticles. *PLoS One*, **4**, e5290.
9. Farjo, R., Skaggs, J., Quiambao, A.B., Cooper, M.J. and Naash, M.I. (2006) Efficient non-viral ocular gene transfer with compacted DNA nanoparticles. *PLoS One*, **1**, e38.
10. Cai, X., Conley, S.M., Nash, Z., Fliesler, S.J., Cooper, M.J. and Naash, M.I. (2010) Gene delivery to mitotic and postmitotic photoreceptors via compacted DNA nanoparticles results in improved phenotype in a mouse model of retinitis pigmentosa. *FASEB J.*, **24**, 1178–1191.
11. Koirala, A., Makkia, R.S., Cooper, M.J. and Naash, M.I. (2011) Nanoparticle-mediated gene transfer specific to retinal pigment epithelial cells. *Biomaterials*, **32**, 9483–9493.
12. Padegimas, L., Kowalczyk, T.H., Adams, S., Gedeon, C.R., Oette, S.M., Dines, K., Hyatt, S.L., Sesenoglu-Laird, O., Tyr, O., Moen, R.C. *et al.* (2012) Optimization of hCFTR lung expression in mice using DNA nanoparticles. *Mol. Ther.*, **20**, 63–72.
13. Yurek, D.M., Flectcher, A.M., Kowalczyk, T.H., Padegimas, L. and Cooper, M.J. (2009) Compacted DNA nanoparticle gene transfer of GDNF to the rat striatum enhances the survival of grafted fetal dopamine neurons. *Cell Transplant.*, **18**, 1183–1196.
14. Yurek, D.M., Fletcher, A.M., McShane, M., Kowalczyk, T.H., Padegimas, L., Weatherspoon, M.R., Kaytor, M.D., Cooper, M.J. and Ziady, A.G. (2011) DNA nanoparticles: detection of long-term transgene activity in brain using bioluminescence imaging. *Mol. Imaging*, **10**, 327–339.
15. Yurek, D.M., Fletcher, A.M., Smith, G.M., Seroogy, K.B., Ziady, A.G., Molter, J., Kowalczyk, T.H., Padegimas, L. and Cooper, M.J. (2009) Long-term transgene expression in the central nervous system using DNA nanoparticles. *Mol. Ther.*, **17**, 641–650.
16. Ziady, A.G., Gedeon, C.R., Miller, T., Quan, W., Payne, J.M., Hyatt, S.L., Fink, T.L., Muhammad, O., Oette, S., Kowalczyk, T. *et al.* (2003) Transfection of airway epithelium by stable PEGylated poly-L-lysine DNA nanoparticles *in vivo*. *Mol. Ther.*, **8**, 936–947.
17. Ziady, A.G., Gedeon, C.R., Muhammad, O., Stillwell, V., Oette, S.M., Fink, T.L., Quan, W., Kowalczyk, T.H., Hyatt, S.L., Payne, J. *et al.* (2003) Minimal toxicity of stabilized compacted DNA nanoparticles in the murine lung. *Mol. Ther.*, **8**, 948–956.
18. Ding, X.Q., Quiambao, A.B., Fitzgerald, J.B., Cooper, M.J., Conley, S.M. and Naash, M.I. (2009) Ocular delivery of compacted DNA-nanoparticles does not elicit toxicity in the mouse retina. *PLoS One*, **4**, e7410.
19. Han, Z., Koirala, A., Makkia, R., Cooper, M.J. and Naash, M.I. (2012) Direct gene transfer with compacted DNA nanoparticles in retinal pigment epithelial cells: expression, repeat delivery and lack of toxicity. *Nanomedicine (Lond.)*, **4**, 521–539.
20. Jackson, D.A., Juranek, S. and Lipps, H.J. (2006) Designing nonviral vectors for efficient gene transfer and long-term gene expression. *Mol. Ther.*, **14**, 613–626.
21. Heng, H.H., Goetze, S., Ye, C.J., Liu, G., Stevens, J.B., Bremer, S.W., Wykes, S.M., Bode, J. and Krawetz, S.A. (2004) Chromatin loops are selectively anchored using scaffold/matrix-attachment regions. *J. Cell Sci.*, **117**, 999–1008.
22. Stehle, I.M., Scinteie, M.F., Baiker, A., Jenke, A.C. and Lipps, H.J. (2003) Exploiting a minimal system to study the epigenetic control of DNA replication: the interplay between transcription and replication. *Chromosome Res.*, **11**, 413–421.
23. Bode, J., Benham, C., Knopp, A. and Mielke, C. (2000) Transcriptional augmentation: modulation of gene expression by scaffold/matrix-attached regions (S/MAR elements). *Crit. Rev. Eukaryot. Gene Expr.*, **10**, 73–90.
24. Rupprecht, S. and Lipps, H.J. (2009) Cell cycle dependent histone dynamics of an episomal non-viral vector. *Gene*, **439**, 95–101.
25. Jenke, B.H., Fetzer, C.P., Stehle, I.M., Jonsson, F., Fackelmayer, F.O., Conradt, H., Bode, J. and Lipps, H.J. (2002) An episomally replicating vector binds to the nuclear matrix protein SAF-A *in vivo*. *EMBO Rep.*, **3**, 349–354.
26. Jenke, A.C., Eisenberger, T., Baiker, A., Stehle, I.M., Wirth, S. and Lipps, H.J. (2005) The nonviral episomal replicating vector pEPI-1 allows long-term inhibition of bcr-abl expression by shRNA. *Hum. Gene Ther.*, **16**, 533–539.
27. Papapetrou, E.P., Ziros, P.G., Micheva, I.D., Zoumbos, N.C. and Athanassiadou, A. (2006) Gene transfer into human hematopoietic progenitor cells with an episomal vector carrying an S/MAR element. *Gene Ther.*, **13**, 40–51.
28. Wong, S.P., Argyros, O., Coutelle, C. and Harbottle, R.P. (2011) Non-viral S/MAR vectors replicate episomally *in vivo* when provided with a selective advantage. *Gene Ther.*, **18**, 82–87.
29. Bemelmans, A.P., Kostic, C., Crippa, S.V., Hauswirth, W.W., Lem, J., Munier, F.L., Seeliger, M.W., Wenzel, A. and Arsenijevic, Y. (2006) Lentiviral gene transfer of RPE65 rescues survival and function of cones in a mouse model of Leber congenital amaurosis. *PLoS Med.*, **3**, e347.
30. Chen, Y., Moiseyev, G., Takahashi, Y. and Ma, J.X. (2006) RPE65 gene delivery restores isomerohydrolase activity and prevents early cone loss in Rpe65$^{-/-}$ mice. *Invest. Ophthalmol. Vis. Sci.*, **47**, 1177–1184.
31. Lai, C.M., Yu, M.J., Brankov, M., Barnett, N.L., Zhou, X., Redmond, T.M., Narfstrom, K. and Rakoczy, P.E. (2004) Recombinant adeno-associated virus type 2-mediated gene delivery into the Rpe65$^{-/-}$ knockout mouse eye results in limited rescue. *Genet. Vaccines Ther.*, **2**, 3.
32. Dejneka, N.S., Surace, E.M., Aleman, T.S., Cideciyan, A.V., Lyubarsky, A., Savchenko, A., Redmond, T.M., Tang, W., Wei, Z., Rex, T.S. *et al.* (2004) *In utero* gene therapy rescues vision in a murine model of congenital blindness. *Mol. Ther.*, **9**, 182–188.
33. Cideciyan, A.V. (2010) Leber congenital amaurosis due to RPE65 mutations and its treatment with gene therapy. *Prog. Retin. Eye Res.*, **29**, 398–427.
34. Redmond, T.M., Yu, S., Lee, E., Bok, D., Hamasaki, D., Chen, N., Goletz, P., Ma, J.X., Crouch, R.K. and Pfeifer, K. (1998) Rpe65 is necessary for production of 11-cis-vitamin A in the retinal visual cycle. *Nat. Genet.*, **20**, 344–351.
35. Znoiko, S.L., Rohrer, B., Lu, K., Lohr, H.R., Crouch, R.K. and Ma, J.X. (2005) Downregulation of cone-specific gene expression and degeneration of cone photoreceptors in the Rpe65$^{-/-}$ mouse at early ages. *Invest. Ophthalmol. Vis. Sci.*, **46**, 1473–1479.
36. Mishima, H. and Kondo, K. (1981) Ultrastructure of age changes in the basal infoldings of aged mouse retinal pigment epithelium. *Exp. Eye Res.*, **33**, 75–84.
37. Pang, J.J., Chang, B., Hawes, N.L., Hurd, R.E., Davisson, M.T., Li, J., Noorwez, S.M., Malhotra, R., McDowell, J.H., Kaushal, S. *et al.* (2005) Retinal degeneration 12 (rd12): a new, spontaneously arising mouse

model for human Leber congenital amaurosis (LCA). *Mol. Vis.*, **11**, 152–162.
38. Ekesten, B., Gouras, P. and Salchow, D.J. (2001) Ultraviolet and middle wavelength sensitive cone responses in the electroretinogram (ERG) of normal and Rpe65 $^{-/-}$ mice. *Vision Res.*, **41**, 2425–2433.
39. Li, X., Li, W., Dai, X., Kong, F., Zheng, Q., Zhou, X., Lu, F., Chang, B., Rohrer, B., Hauswirth, W.W. *et al.* (2011) Gene therapy rescues cone structure and function in the 3-month-old rd12 mouse: a model for midcourse RPE65 leber congenital amaurosis. *Invest. Ophthalmol. Vis. Sci.*, **52**, 7–15.
40. Han, z., Conley, S.M., Makkia, R.S., Cooper, M.J. and Naash, M.I. (2012) DNA nanoparticle-mediated ABCA4 delivery rescues Stargardt's dystrophy in mice. *J. Clin. Invest.*, **122**, 3221–3226.
41. Mayerson, P.L. and Hall, M.O. (1986) Rat retinal pigment epithelial cells show specificity of phagocytosis *in vitro*. *J. Cell Biol.*, **103**, 299–308.
42. Chen, X., Kube, D.M., Cooper, M.J. and Davis, P.B. (2008) Cell surface nucleolin serves as receptor for DNA nanoparticles composed of pegylated polylysine and DNA. *Mol. Ther.*, **16**, 333–342.
43. Chen, X., Shank, S., Davis, P.B. and Ziady, A.G. (2011) Nucleolin-mediated cellular trafficking of DNA nanoparticle is lipid raft and microtubule dependent and can be modulated by glucocorticoid. *Mol. Ther.*, **19**, 93–102.
44. Barker, S.E., Broderick, C.A., Robbie, S.J., Duran, Y., Natkunarajah, M., Buch, P., Balaggan, K.S., MacLaren, R.E., Bainbridge, J.W., Smith, A.J. *et al.* (2009) Subretinal delivery of adeno-associated virus serotype 2 results in minimal immune responses that allow repeat vector administration in immunocompetent mice. *J. Gene Med.*, **11**, 486–497.
45. Maeda, T., Maeda, A., Casadesus, G., Palczewski, K. and Margaron, P. (2009) Evaluation of 9-cis-retinyl acetate therapy in Rpe65$^{-/-}$ mice. *Invest. Ophthalmol. Vis. Sci.*, **50**, 4368–4378.
46. Batten, M.L., Imanishi, Y., Tu, D.C., Doan, T., Zhu, L., Pang, J., Glushakova, L., Moise, A.R., Baehr, W., Van Gelder, R.N. *et al.* (2005) Pharmacological and rAAV gene therapy rescue of visual functions in a blind mouse model of Leber congenital amaurosis. *PLoS Med.*, **2**, e333.
47. Han, Z., Koirala, A., Makkia, R., Cooper, M.J. and Naash, M.I. (2012) Direct gene transfer with compacted DNA nanoparticles in retinal pigment epithelial cells: expression, repeat delivery and lack of toxicity. *Nanomedicine (Lond).*, **7**, 521–539
48. Liu, G., Li, D., Pasumarthy, M.K., Kowalczyk, T.H., Gedeon, C.R., Hyatt, S.L., Payne, J.M., Miller, T.J., Brunovskis, P., Fink, T.L. *et al.* (2003) Nanoparticles of compacted DNA transfect postmitotic cells. *J. Biol. Chem.*, **278**, 32578–32586.
49. Chakraborty, D., Conley, S.M., Stuck, M.W. and Naash, M.I. (2010) Differences in RDS trafficking, assembly and function in cones versus rods: insights from studies of C150S-RDS. *Hum. Mol. Genet.*, **19**, 4799–4812.
50. Zhu, X., Brown, B., Li, A., Mears, A.J., Swaroop, A. and Craft, C.M. (2003) GRK1-dependent phosphorylation of S and M opsins and their binding to cone arrestin during cone phototransduction in the mouse retina. *J. Neurosci.*, **23**, 6152–6160.